The Journal of Experimental Biology 204, 185–198 (2001)
Printed in Great Britain © The Company of Biologists Limited 2001
JEB2935

ELECTRORECEPTION IN *GYMNOTUS CARAPO*: DIFFERENCES BETWEEN SELF-GENERATED AND CONSPECIFIC-GENERATED SIGNAL CARRIERS

PEDRO A. AGUILERA, MARÍA E. CASTELLÓ AND ANGEL A. CAPUTI*

Laboratorio de Neurofisiología Comparada, Departamento de Neuroanatomía Comparada, Unidad Asociada a Facultad de Ciencias, Instituto de Investigaciones Biológicas Clemente Estable, Av. Italia 3318, Montevideo, Uruguay

*e-mail: angel@iibce.edu.uy

Accepted 27 October 2000; published on WWW 3 January 2001

Summary

Local electric fields generated by the electric organ discharge of *Gymnotus carapo* were explored at selected points on the skin of an emitter fish ('local self-generated fields') and on the skin of a conspecific ('local conspecific-generated fields') using a specially designed probe. Local self-generated fields showed a constant pattern along the body of the fish. At the head, these fields were collimated, much stronger than elsewhere on the fish, and had a time waveform that was site-independent. This waveform consisted of a slow head-negative wave followed by a faster head-positive wave. In contrast, time waveforms in the trunk and tail regions were site-specific, with field vectors that changed direction over time. Local conspecific-generated fields were similar to the head-to-tail field, but their spatio-temporal pattern at the skin depended on the relative orientation between the receiving fish and the emitting fish. Because self-generated fields had a slow early component at the head region, they displayed a low-frequency peak in their power spectral density histograms. In contrast, the conspecific-generated fields had time waveforms with a sharper phase reversal, resulting in a peak at higher frequency than in the self-generated field. Lesions in emitting fish demonstrated that waveform components generated by the trunk and tail regions of the electric organ predominate in conspecific-generated fields, whereas waveform components generated by the abdominal region prevail in self-generated fields. Similar results were obtained from *Brachyhypopomus pinnicaudatus*. These results suggest that, in pulse-emitting gymnotids, electrolocation and electrocommunication signals may be carried by different field components generated by different regions of the electric organ.

Key words: electrocommunication, electroreception, electric organ discharge, pre-receptor mechanism, gymnotid, *Gymnotus carapo*, *Brachyhypopomus pinnicaudatus.*

Introduction

Sensory signals can be considered as the modulations of a specific 'carrier' for which the sensory system has specific sensitivity (Wiener, 1948). Vision is a paradigmatic example that allowed Marr (Marr, 1982) to define the main factors that determine physical image generation, considering light as the carrier of visual information. Two of these factors are the illuminating conditions and the observer's viewpoint. Just as light is necessary for vision, so the presence of a specific carrier is necessary for any other sensory system. To understand how a sensory system works, one has to characterise the carrier that holds the signals processed by that system.

This paper is concerned with the signal carriers of the electrosensory system, a peculiar active sensory system that allows electric fish to communicate with each other and to explore their near environment through electric signals (Lissmann and Machin, 1958; Black-Cleworth, 1970). The carriers of these signals are the electric fields generated by activation of the electric organ that transform the body of the fish into a distributed electric source. When loaded by a surrounding impedance (the water), the electric organ discharge (EOD) generates spatio-temporal patterns of current density that flow through the skin of the emitter fish and, potentially, through the skin of nearby conspecifics (Caputi, 1999).

Active electrolocation occurs when the self-generated electric field is used to image the near environment. Objects of different impedance from water interfere with the self-generated electric field and modulate the basal pattern of transcutaneous currents. The intensity of this field at a given point of the skin is a vector, referred to here as the self-generated local EOD-associated field (sLEOD). Theoretical considerations and experimental data indicate that the heterogeneous electric organs of pulse-emitting gymnotids generate sLEODs with time waveforms that are strongly dependent on their spatial coordinates along the body of the fish (Bastian, 1977; Watson and Bastian, 1979; Trujillo-Cenóz et al., 1984; Caputi et al., 1989; Caputi et al., 1994; Caputi et al., 1998b; Caputi and Budelli, 1995; Caputi, 1999; Assad et

al., 1999; Stoddard et al., 1999). Thus, to understand how objects generate electric images, it is essential to study the basal carrier (sLEOD) at different sites on the skin, particularly in those regions of skin with a high density of electroreceptors.

Electrocommunication is the transmission of electric signals between fish. The natural carriers for electrocommunication are the EOD-associated electric fields generated by neighbouring conspecifics (the conspecific-generated local EOD-associated field, cLEOD). The time waveforms of these fields depend not only on the heterogeneous waveforms of the emitted pattern, but also on the 'viewpoint' of the receiving fish (i.e. its orientation relative to the emitting fish).

As a corollary, it can be predicted that the time waveform of an sLEOD recorded at a given point on the emitter fish's surface should be different from the time waveform of the cLEOD at the homologous point on the receiving fish. Therefore, the sLEOD and cLEOD should stimulate the same population of electroreceptors in different ways. Despite this important point, differences between the sLEOD and cLEOD have not been studied systematically.

This paper describes the differences between these two kinds of LEOD. To compare them, our study is focused mainly on the peri-oral region. We have previously distinguished an electroreceptive 'fovea' on the surface of the jaw, and a 'parafovea' on the surface of the snout. The peri-oral region exhibits the largest variety and density of electroreceptors and has a major central representation. In addition, pre-receptor processing increases both self-generated and exogenous electric signals within this region (Castelló et al., 1998; Castelló et al., 2000).

Our results show that the sLEOD displays a biphasic waveform at the fovea of the emitter fish, whereas the cLEOD can be described generally as a triphasic waveform, similar to the head-to-tail EOD (htEOD). Neural and electric organ lesions altering the EOD demonstrated that the sLEOD is generated mainly by the abdominal region of the electric organ, while the cLEOD is generated mainly by the trunk and tail regions of the electric organ. We conclude that active electrolocation and electrocommunication signals may be carried by different components of the EOD.

Materials and methods

General

Fifty, non-sexually differentiated, *Gymnotus carapo* (L.) and two male *Brachyhypopomus pinnicaudatus* (Hopkins, 1991) were used in this study. All surgery was performed under anaesthesia, and experiments were conducted following the IIBCE's rules for the use of experimental animals and the guidelines of the Society for Neuroscience.

Measurements and representation of EOD-associated fields

Electric fields produced by the EOD were recorded in two different ways: (i) using two electrodes, one close to the head and the other close to the tail. This gave an htEOD with four wave components (V_1–V_4; described by Trujillo-Cenóz et al., 1984) (see Fig. 1A for an example) and (ii) using a specially designed probe placed close to the skin of the fish at different points along its body (LEOD). The latter technique (described in detail by Castelló et al., 2000) was used to record local potential gradients equivalent to orthogonal components of the local electric field vector at that point. We recorded LEODs at selected points on the skin either in the emitting fish (self-generated LEOD, sLEOD) or in a neighbouring conspecific (conspecific-generated LEOD, cLEOD).

The LEODs were measured under two experimental conditions: (i) in intact animals and (ii) in animals whose EOD had been partially silenced by selective lesions of electric organ or its electromotor supply. Fish were restrained within a net in the centre of a 32 cm×21 cm×8 cm tank filled with water. The conductivity of the surrounding water (220–240 $\mu S\,cm^{-1}$) was selected on the basis of the mean annual conductivity of the fishes' natural habitat (A. C. Silva, personal communication). To compare the LEOD at the skin with local fields occurring in the nearby water, the same types of measurement were performed at different distances from the skin. LEODs were measured using four electrodes assembled into a single probe (Castelló et al., 2000). The probe was constructed from four nichrome wires insulated except at their tips (200 μm thick, impedance approximately 50 kΩ). Active electrodes were oriented along orthogonal axes (longitudinal *x*, lateral *y* and vertical *z*) intersecting at the same point. Their tips were 2 mm from the intersection of the axes, where the tip of the fourth wire (reference electrode) was located. The axes of the probe were placed parallel to the homologous axes of the fish, with the reference electrode just in the front of the point on the skin to be explored. To compare the sLEOD and cLEOD, particular attention was paid to the foveal region.

The voltage difference between each of the active electrodes and the reference electrode was measured using a high-input-impedance, high-gain differential amplifier (10 Hz to 10 kHz band-pass filter). Recorded waveforms were displayed, averaged (8–64 sweeps) and measured using a digital oscilloscope. Digital data were transferred to a computer for off-line processing.

Voltage measurements (v_{xr}, v_{yr} and v_{zr}) were considered to be proportional to the voltage gradient along the orthogonal axes and, therefore, to the vector components of the LEOD ($\mathbf{LEOD_x}$, $\mathbf{LEOD_y}$, $\mathbf{LEOD_z}$). Vectorial addition of these components results in the LEOD:

$$\mathbf{LEOD} = \mathbf{LEOD_x} + \mathbf{LEOD_y} + \mathbf{LEOD_z}, \quad (1)$$

The proportionality constant between the measured voltage difference and the voltage gradient depended on the distance between the active and reference electrodes and on the eccentricity of the reference electrode caused by construction constraints. Each local field orthogonal component was expressed in $V\,cm^{-1}$ (thus, $\mathbf{LEOD_x}=\mathbf{v_{xr}}*5$, $\mathbf{LEOD_y}=\mathbf{v_{yr}}*5$ and $\mathbf{LEOD_z}=\mathbf{v_{zr}}*5$). Since more than one probe was used for the experiments, trigonometric calculations were applied to compensate the error when eccentricity was significant.

The modulus and angles of the local field vector at the point explored were calculated as a function of time using basic trigonometry (equations 2, 3 and 4).

$$\text{Modulus (time)} = \sqrt{\mathbf{LEOD_x(time)^2 + LEOD_y(time)^2 + LEOD_z(time)^2}}, \quad (2)$$

$$\text{Azimuth (time)} = \mathbf{arctan}\,\frac{\mathbf{LEOD_y(time)}}{\mathbf{LEOD_x(time)}}, \quad (3)$$

$$\text{Elevation (time)} = \mathbf{arctan}\,\frac{\mathbf{LEOD_z(time)}}{\mathbf{LEOD_x(time)}}, \quad (4)$$

Because the local fields studied are vectorial quantities, they are represented in the following ways: (i) as vector loops (the trajectory of vector angles and modulus), (ii) as vector orthogonal components as a function of time, (iii) as time waveforms and (iv) as power spectral density histograms. Vector loops are two-dimensional or three-dimensional Cartesian representations of the LEOD vector at all the sampled times. The axes of these plots correspond to the Euclidean spatial directions. Vector orthogonal components are shown as functions of time in Cartesian plots (as superimposed traces of different colour). At the fish's head, the sLEOD was perpendicular to the skin throughout the EOD and the same was true for the cLEOD at the fovea. In these conditions, an LEOD was equal to the product of its modulus and a one-dimensional vector representing its direction. The direction vector was −1 when the outside of the fish was positive with respect to the inside, and +1 in the opposite case. We refer to such representations as time waveforms (see red trace in Fig. 1B for an example). In some cases, time waveforms were normalised to their peaks (V_3) when we were interested in comparing the waveforms of several recordings. The time waveforms of these LEODs perpendicular to the skin are the effective stimuli for electroreceptors, so it was useful to show them in the frequency domain also (power spectral density). The power spectral density histograms of the time waveforms were calculated as the absolute value of the Fast Fourier Transform and normalised to their peaks for ease of comparison.

Using the same general procedure, cLEODs generated by a conspecific (emitting fish) placed in the same tank, were recorded. Different pairs of fish at different orientations were explored.

A necessary condition for a carrier of electrolocation signals is for it to be distorted by nearby objects or local conductance inhomogeneities, so we verified this for the sLEOD. The effect of short circuits between two points in front of the fovea was studied in five fish. Two wires, insulated except at their tips, were placed in front of the probe along the sagittal axis; one of the wires was 0.5 cm and the other 3 cm from the skin. The wires could be connected at will by an external switch, and the sLEOD recorded while short-circuiting the wires was compared with the sLEOD recorded with the circuit open.

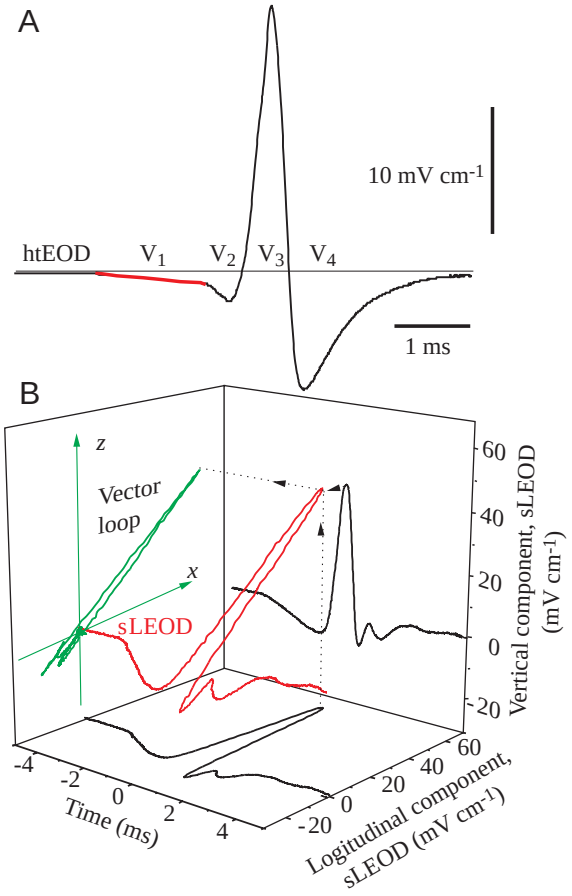

Fig. 1. (A) The head-to-tail electric-organ-discharge-associated field (htEOD) recorded between an electrode close to the head and another close to the tip of the tail (average of eight sweeps) of *Gymnotus carapo*. The wave components (terminology according to Trujillo-Cenóz et al., 1984) have been labelled [V_1 (red), V_2, V_3 and V_4]. (B) A plot showing the relationships between some of the different displays used in this paper. Local electric-organ-discharge-associated field (LEOD) components were recorded at selected points on the skin, and the LEOD waveform was calculated as a function of time (see Materials and methods). In this example, the data were obtained with the electrode placed at the midline, so the lateral local field component is virtually absent and is excluded from the representation for the sake of clarity. The third dimension has been used to represent time; ordinates are along the corresponding spatial directions. The black trace in the vertical plane corresponds to the vertical self-generated LEOD (sLEOD) component plotted as a function of time (average of eight sweeps). The black trace in the horizontal plane corresponds to the longitudinal sLEOD component as a function of time (average of eight sweeps). Dotted lines indicate how pairs of data obtained simultaneously at the peak of V_3 determine the amplitude and orientation of the corresponding local field vector at this time (peak points on the red and green traces). The local field obtained using this procedure is plotted over time in red (the time waveform, labelled sLEOD) and as a vector loop in green (projected onto the sagittal plane defined by the *x* and *z* axes).

Recordings of sLEODs and cLEODs generated by fish with partially silenced electric organs

In a second type of experiment, the LEOD generated by selected regions of the electric organ was studied. The recording procedures described above were repeated before and after spinal section or abdominal surgery. Spinal section was used to abolish the trunk- and tail-generated EOD (five fish). The spinal cord was exposed by a laminectomy and severed between the rostral and middle thirds of the fish. Surgical resection of the abdominal portion of the electric organ was used to abolish the abdomen-generated EOD (five fish; Trujillo-Cenóz et al., 1984). The abdominal portion of the electric organ was exposed by making a longitudinal incision along the midline, and abdominal electrocytes were destroyed one by one using fine forceps.

Electromotoneuron pools that innervate different regions of the electric organ (Caputi and Trujillo-Cenóz, 1994) are distributed within overlapping regions of the spinal cord, so spinal lesions either left a remnant of V_3 at the abdominal region or caused a decay of V_3 beyond the limits of the abdominal region. Despite this limitation, spinal lesions could be used to study the origin of LEODs by checking the remaining electromotive forces corresponding to each portion of the electric organ.

Recording the electromotive force generated by different regions of the electric organ

The air-gap technique (Caputi et al., 1989; Caputi et al., 1993; Caputi et al., 1994; Caputi et al., 1998b) was employed to verify the success of the surgery in both cases. The voltage drop generated by different portions of the fish's body when isolated in air was recorded as follows: fish were suspended in air using a net, and three wires were placed in contact with the skin perpendicular to the main axis of the body, one at each extreme of the fish and the third at the caudal limit of the abdomen. Voltages recorded between pairs of these wires were generated by the trunk and tail, by the abdominal region or by the sum of both activities (head-to-tail electromotive force). In the air gap condition, there is no load, so voltage recordings are good estimators of the electromotive forces generated by different portions of the electric organ.

Results

In the following sections, we describe the local EOD-associated fields recorded either at the skin of an emitter fish (sLEOD) or at the skin of a receiving conspecific fish (cLEOD). Theoretical studies (Caputi et al., 1998a; Budelli and Caputi, 2000; Sicardi et al., 2000) indicate that LEODs are proportional to the local transcutaneous current density, which is the natural stimulus for electroreceptors.

We describe LEODs using four different representations: (i) vector loops, (ii) vector orthogonal components as a function of time, (iii) time waveforms, and (iv) power spectral density histograms (see Materials and methods for an explanation). The relationships between some of these different representations are shown in Fig. 1.

The time waveform of the head-to-tail EOD (htEOD) is used as a standard reference throughout. htEOD wave components are referred to as V_1, V_2, V_3 and V_4 (Fig. 1A; terminology of Trujillo-Cenóz et al., 1984). The prefixes 's' (for self-generated) and 'c' (for conspecific) are used to refer to the equivalent wave components of the sLEOD and the cLEOD respectively (e.g. sV_1, sV_3, etc.).

Self-generated local EOD-associated fields (sLEODs)

The orthogonal components (Fig. 2A, black and red upper traces), modulus (Fig. 2A, green lower traces) and vector loops (Fig. 2B) of the sLEOD recorded at the same percentage distance from the head were very similar from fish to fish. For each studied fish (N=5), the local field modulus was greatest at the lower jaw, where the density and variety of electroreceptors is also greatest (the electroreceptive fovea; Castelló et al., 2000). The amplitude of the sLEOD decreased caudally, reaching 30 % of the maximum at the limit of the cranium (10 % of fish length, Fig. 2A green lower traces and Fig. 2B).

Our study of these waveforms and vector loops indicated that, as required for high-resolution image-processing, local fields at the electroreceptive fovea were collimated (i.e. had constant angles) and coherent (i.e. had similar waveforms). In contrast, in the trunk region, vector angles varied with time and time waveforms were site-dependent (Fig. 2). On the head, the local field vector trajectory followed a line perpendicular to the skin. This kind of local field collimation, reported previously for *Gymnotus carapo* (Castelló et al., 2000), also occurs in other gymnotids (Rasnow and Bower, 1996; Stoddard et al., 1999).

In the peri-oral region, sLEODs had similar waveforms, consisting of a slow negative wave (sV_1) followed by a positive peak (sV_3). As a result of collimation, only the magnitude and sign of the field vector changed during the EOD and, therefore, current flowed inwards during sV_1 and outwards during sV_3. For this reason, when dealing with the head region, we calculated and displayed the local field vector perpendicular to the skin, assigning a negative value when current density flowed inwards and a positive value in the opposite case.

Waveform coherency at the electroreceptive fovea is illustrated in Fig. 3, in which 17 sLEOD time waveforms at different positions within the fovea of one fish have been superimposed. Waveform amplitude varied by approximately 20 % between these different sites on the fovea, but the traces have been normalised to the sV_3 peak so that they may be compared more easily. A coefficient of variation for sV_1/sV_3 of 0.25 was found when comparing different sites within the fovea of the same fish. To depict regional differences in this ratio, we compared recordings made at the midline of the lower jaw (fovea) with recordings made at the midline of the snout (parafovea) in 25 fish ranging from 9 to 29 cm in total length. Parafoveal sV_1/sV_3 ratios were slightly, but significantly, larger than foveal sV_1/sV_3 ratios (sV_1/sV_3 at the fovea 0.18±0.04,

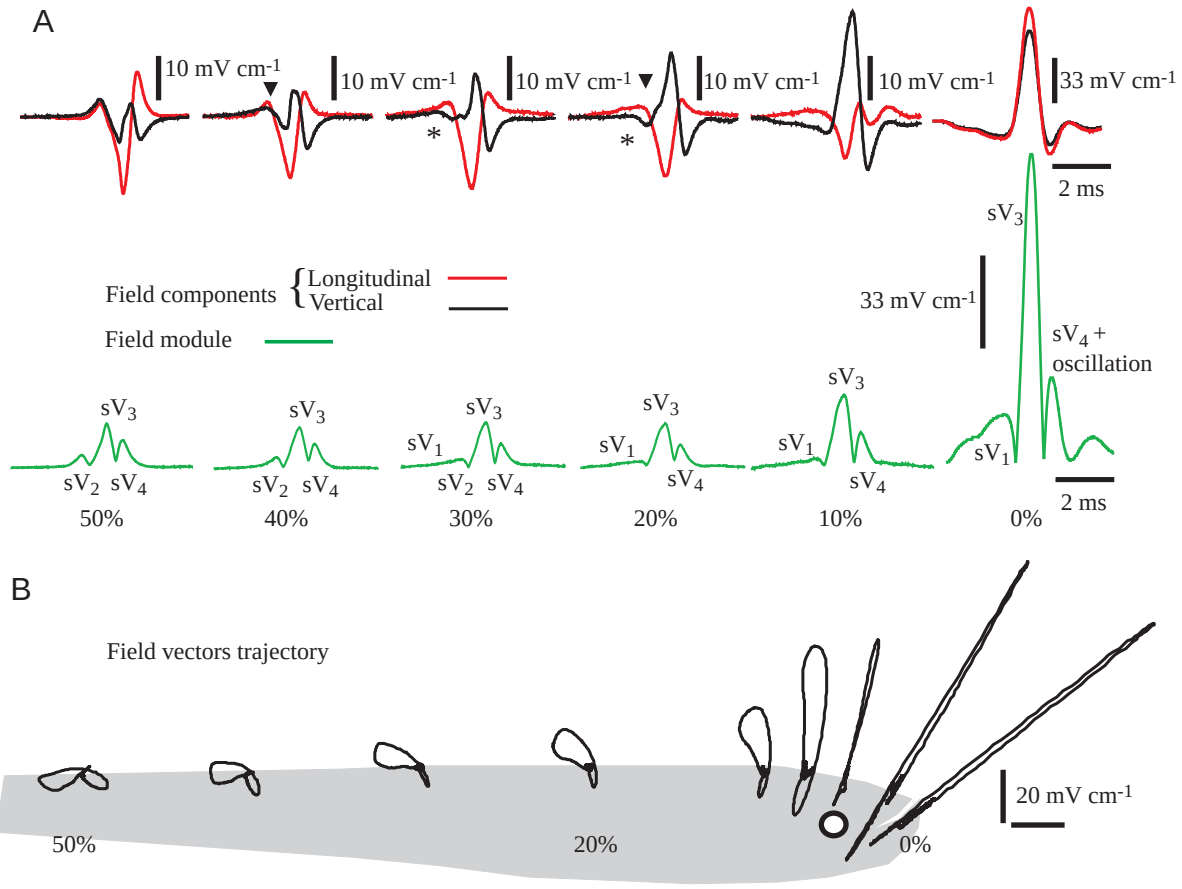

Fig. 2. General view of the spatio-temporal pattern of the self-generated local electric-organ-discharge-associated field (sLEOD). For an explanation of the nomenclature, see Fig. 1. (A) Recordings of vector components along the longitudinal (red traces) and vertical (black traces) axes and the local field modulus (green traces) obtained at six sites along the fish's midline (average of eight sweeps in each case). Distances from the jaw are expressed as a percentage of fish length. (B) Vector trajectories. Note that, in the head region, the local field components are similar (coherent) and therefore vector angles are time-independent. In the trunk region, the sLEOD components are different, so the field vectors describe a loop. For an explanation of asterisks and arrowheads, see text.

sV_1/sV_3 at the parafovea 0.21±0.05; means ± S.D.; N=25; paired sample t-test P<0.001). This indicates that the vertical component of sV_1 relative to sV_3 is larger at the parafovea than at the fovea, as pointed out by Assad et al. (Assad et al., 1999).

When the electrodes were in contact with the skin, a series of small oscillations was recorded following sV_3 (Fig. 3 inset). These oscillations varied in size and waveform, depending on the position of the electrode and respiratory movements, and probably represent the response of the local electroreceptor population to the EOD (Bennett, 1971; Watson and Bastian, 1979).

Within the trunk region, the Cartesian components of the sLEOD exhibited different waveforms; consequently, vector angles described site-specific loops resulting from the different origins of the EOD waveform components. In this region, the longitudinal component of the sLEOD waveform was similar to the htEOD, while the vertical and lateral sLEOD components depended greatly on electrode position. As shown in Fig. 2, vertical components recorded between 10 and 50 % of fish length (black traces in Fig. 2A) were perpendicular to the skin and therefore proportional to the local transcutaneous current density. Analysis of the different deflections of the vertical component (Fig. 2A, black trace) illustrated the following about their different origins: (i) At 20 % and 30 % along the fish's body, an outward sV_1 (asterisk) indicated that external currents at this time in the EOD flow between the rostral trunk and the head; (ii) sV_2 is inward at 20 % along the body but became outward caudal to 40 % (arrowhead); (iii) sV_3, generated all along the electric organ, showed a complex spatial pattern that caused a polyphasic wave at 50 % along the fish's body; (iv) sV_4, generated in the tail, is inward in the rostral 60 % of the fish.

The htEOD results from integration of the longitudinal local fields. Consistently, triphasic recordings indicate that V_3-generating currents flow in the rostral-to-caudal direction while the currents generating the other components flow in the opposite direction (V_1 beside the head, V_2 beside the trunk and V_4 beside the trunk and tail).

A necessary condition for a carrier of electrolocation signals is for it to be modulated by nearby conductance

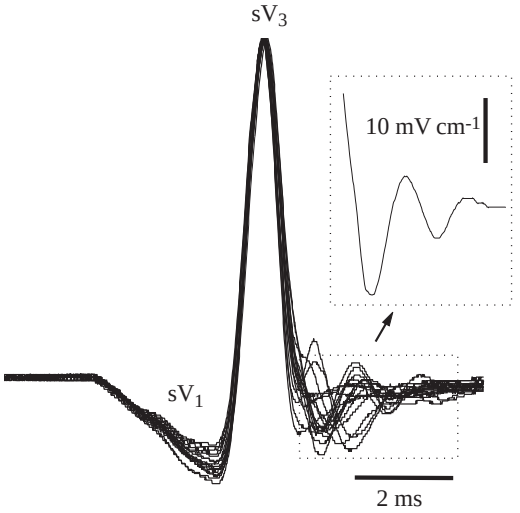

Fig. 3. Waveform coherence of the self-generated local electric-organ-discharge-associated field (sLEOD) at the electrorecepetive fovea. For an explanation of the nomenclature, see Fig. 1. Normalised sLEOD time waveforms (average of eight sweeps) were obtained from 17 different positions located at the intersection of equally spaced parasagittal and transverse lines on the left hemi-foveal region of a single fish. Note that the late oscillations due to the activity of peripheral elements of the electrosensory system vary from site to site but at each site are phase-locked to the sLEOD (a single trace, average of eight sweeps, is shown in detail in the inset).

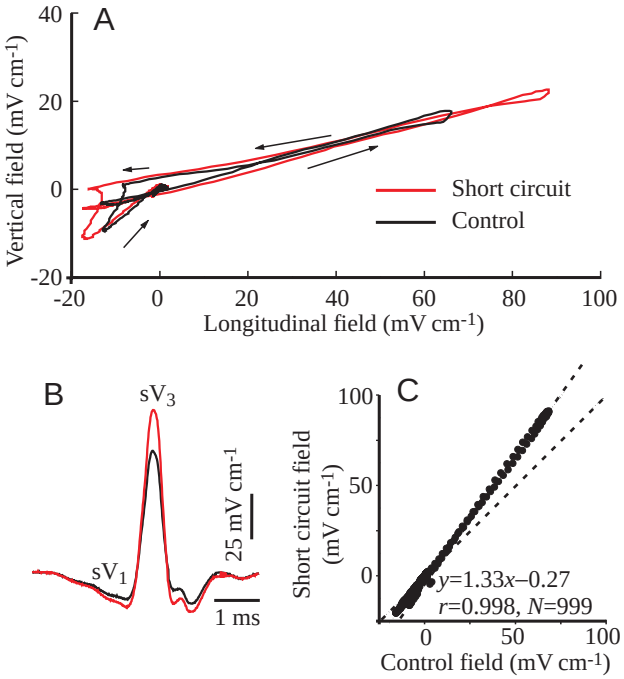

Fig. 4. Modulation of the self-generated local electric-organ-discharge-associated field (sLEOD) by a short circuit. A short circuit between two electrodes 0.5 cm and 3 cm in front of the skin caused changes in the nearby local field. The control condition is represented in black, and the short-circuit condition in red. (A) Local field vector loops of the sLEOD recorded at the midline of the jaw (foveal region) before and during the short circuit (average of eight sweeps). (B) Time waveforms of the sLEOD shown in A (average of eight sweeps). Simultaneous recordings of the head-to-tail electric-organ-discharge-associated field were not affected by the short circuit and were used as the time reference to align the recordings. (C) Short-circuit time waveform plotted against control time waveform. The slope of the line (1.33 in this case) is a measure of the amount of modulation (r=0.998, P<0.001). The reference broken line at 45 ° corresponds to the no-change situation.

inhomogeneities. We investigated this for the sLEOD using a short circuit. As shown in Fig. 4, a longitudinal short circuit between two wires (2.5 cm apart) placed in front of the fovea increased the sLEOD amplitude by 30 %.

Conspecific-generated LEOD waveforms on the skin of a receiving fish

The spatio-temporal pattern of cLEODs in the receiving fish varied with the distance and relative orientation of the emitting fish. The example in Fig. 5 was obtained with the emitter fish placed anti-parallel (the fish were side by side with their heads and tails pointing in opposite directions) and 7 cm lateral to the receiving fish. cLEOD vector trajectories (Fig. 5A) and components (Fig. 5B) obtained at four sites along the midline of the receiving fish are shown. When fish were side by side (parallel or anti-parallel), the amplitude of the cLEOD was largest at the fovea and gradually decayed caudally, as occurred with the sLEOD. The amplitude of the cLEOD diminished when the electrode was moved away from the fish, indicating that current density increases in the vicinity of the electroreceptive fovea. In the example shown, the cLEOD at the fovea was 1.4 times larger than the local field recorded 4 mm away from the skin. This local field enhancement is due to the ‘funnelling effect’ (see Castelló et al., 2000).

In general, cLEOD waveforms showed the same sequence of wave components (described as cV_1–cV_2–cV_3–cV_4) as the htEOD (Figs 6, 7). This sequence was present in most cLEOD recordings for relatively well-separated fish (in general, more than 1 body length from the emitter fish); however, variations in the ratios cV_2/cV_3 and cV_3/cV_4 within the range ±50 % around the equivalent ratios of the htEOD were observed. These variations depended on the relative orientation of the fish (Figs 6, 7) and their relative sizes (Figs 8, 9). Despite these variations, the power spectral density histograms of the cLEOD and the htEOD were similar, although the peak frequency of the cLEOD histogram was often shifted to higher frequencies because of the increased slope of its temporal waveform at polarity transitions (Figs 6, 10).

The foveal cLEOD was studied systematically as a function of distance in four fish, in both parallel and anti-parallel orientations. The amplitude of the foveal cLEODs was always smaller than the amplitude of the foveal sLEODs, irrespective of relative fish orientation. In each case, cLEOD amplitudes and waveforms were dependent on the distance between and relative orientation of the fish (Fig. 7). The amplitude of the

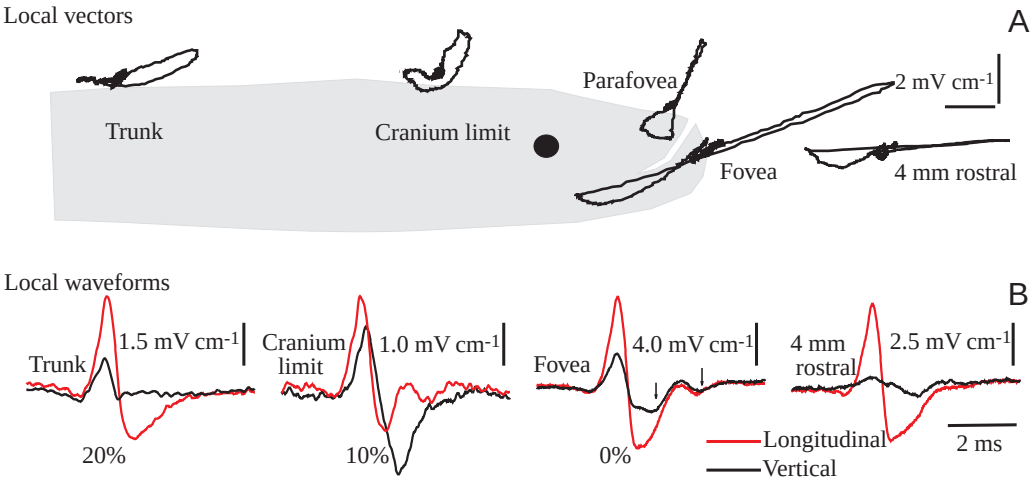

Fig. 5. General view of the spatio-temporal pattern of the conspecific-generated local electric-organ-discharge-associated field (cLEOD) at the midline of a receiving fish, when the emitter fish was placed antiparallel and 7 cm away. Vector trajectories (single sweeps, A) and LEOD longitudinal (red) and vertical (black) components (single sweeps, B) obtained at four sites adjacent to the skin are compared with the components of the local field obtained when the electrode was placed 4 mm away from the skin. Recording sites are as marked; distances from the fovea are measured as a percentage of fish length. Arrows mark the oscillations generated by the electroreceptor responses to the cLEOD.

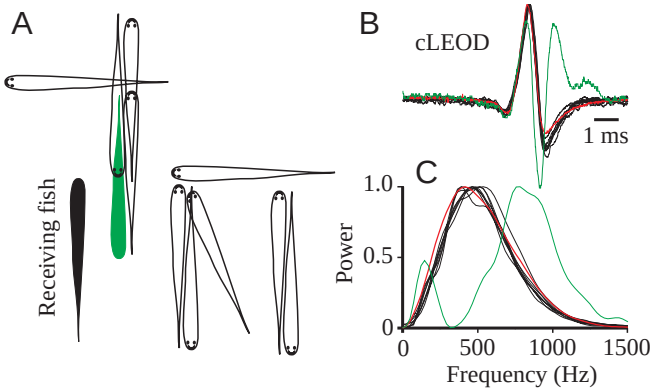

Fig. 6. The normalised conspecific-generated local electric-organ-discharge-associated field (cLEOD) generated by an emitter fish 14 cm long (black outline fishs) at the fovea of a receiving fish 12 cm long (black solid fish); an average of eight sweeps in each case. Eleven different orientations shown diagramatically in A are compared in this example. Foveal cLEODs represented by their normalised time waveforms (B) and their normalised power spectral density histograms (C). Note the similarity of waveforms and power spectral densities between the cLEOD (black lines) and the head-to-tail electric-organ-discharge-associated field (red lines). Interestingly, when the emitter fish was positioned as represented by the 'green' fish in A, the waveform (green line and spectrum plot) was very different from waveforms obtained at other orientations.

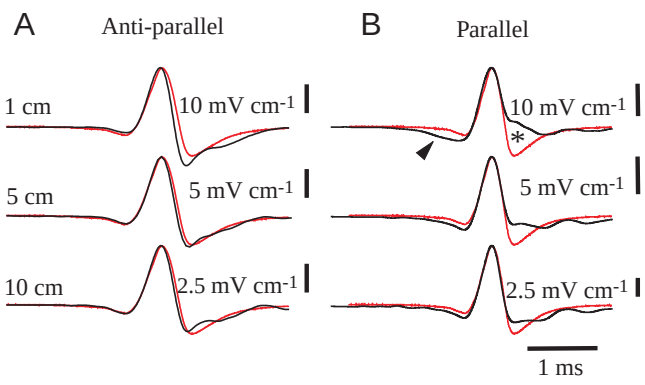

Fig. 7. Normalised conspecific-generated local electric-organ-discharge-associated field (cLEOD) (black) in anti-parallel (A) and parallel (B) oriented fish, with the head-to-tail electric-organ-discharge-associated field of the emitter fish (red) for comparison. Each trace is the average of eight sweeps. Time waveforms of cLEOD amplitude at the fovea of a 12 cm long receiving fish generated by a 15 cm long emitter fish at three different distances from the receiving fish (1 cm, 5 cm and 10 cm). Only when the fish were parallel and very close to each other was cV_1 obvious (arrowhead) and cV_4 practically absent (asterisk); for an explanation of the nomenclature see Fig. 1.

foveal cLEOD increased with length of the emitter fish and decreased with the distance between fish (Fig. 8). cV_2 at the electroreceptive fovea was larger in parallel than in anti-parallel fish (Fig. 8A,D). In contrast, cV_3 and cV_4 were larger in anti-parallel fish than in parallel fish (Fig. 8B,C,E,F). The differences between parallel and anti-parallel fish were more marked for cV_4 and cV_2 than for cV_3. For anti-parallel fish, the amplitude of cV_3 and cV_4 decreased more rapidly with distance than for parallel fish, while in most cases the opposite occurred for cV_2 (Fig. 8). Waveforms also changed consistently with distance (Figs 7, 9).

The ratio cV_2/cV_3 depended on both the distance and the size of the emitter fish. For a small emitting fish (Fig. 9A, 7.5 cm long), cV_2/cV_3 increased with distance in both the parallel and anti-parallel orientation. For an intermediate-sized emitting fish (Fig. 9B, 10.5 cm long), there was no clear change in this variable with distance. For a large emitting fish (15 and 19.5 cm length), cV_2/cV_3 increased with distance in the anti-

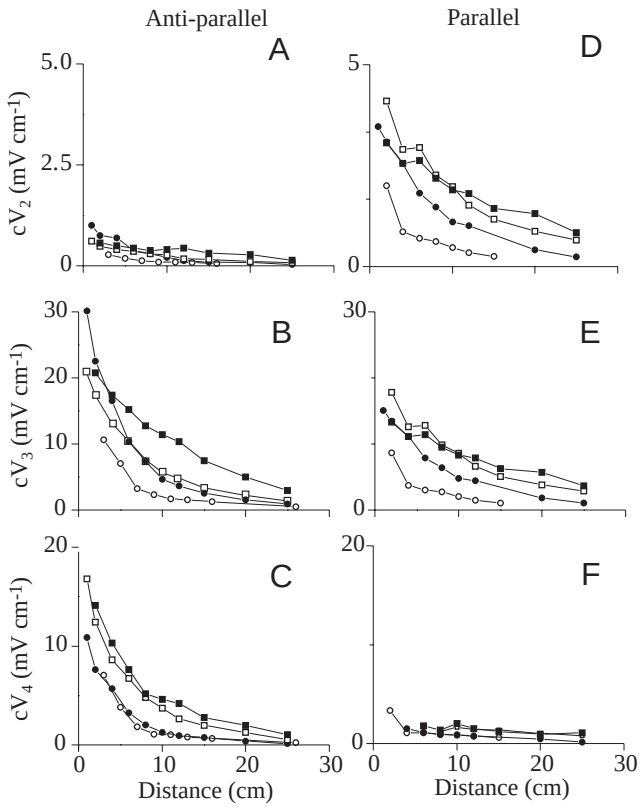

Fig. 8. Peak amplitudes of different time waveform components of the conspecific-generated local electric-organ-discharge-associated field (cLEOD) plotted as a function of distance between fish positioned anti-parallel and parallel. Emitter fish lengths: 7.5 cm (○), 11 cm (●), 15 cm (□) and 19.5 cm (■). Receiving fish length, 12 cm. (A) cV_2, anti-parallel fish; (B) cV_3, anti-parallel fish; (C) cV_4, anti-parallel fish; (D) cV_2, parallel fish; (E) cV_3, parallel fish; (F) cV_4, parallel fish. Note the different effects of anti-parallel and parallel orientations on cV_2 and cV_4. For an explanation of the nomenclature, see Fig. 1.

parallel orientation but decreased with distance in the parallel orientation (Fig. 9C,D).

The ratio cV_4/cV_3 showed a more consistent dependence on distance as fish size varied. This ratio decreased with distance in anti-parallel orientations and increased with distance in parallel orientations, irrespective of the size of the emitting fish, and tended to be equal in parallel and anti-parallel orientations when the fish were far apart (more than 1.5 body lengths between the fish; Fig. 9E–H).

Exceptions to the cV_1–cV_2–cV_3–cV_4 sequence were observed when the distance between the fish was less than 1 body length of the emitter fish with the abdominal zones overlapping. A systematic study of cLEOD waveform as a function of relative fish size, distance and orientation is still not complete (P. Aguilera, M. E. Castelló, A. A. Caputi, in preparation). Therefore, only two instructive examples are reported here (Figs 6, 7B). The example represented by the green fish and traces in Fig. 6 was one of the clearest cases in which the cLEOD differed from the usual pattern. In this example, the fish were close to each other and anti-parallel, with their abdominal regions overlapping (Fig. 6A); the cLEOD was polyphasic, and its power spectrum density histogram showed two peaks at frequencies very different from the cLEODs recorded with the fish in other orientations (green traces in Fig. 6B,C). Note that, when the fish were in the same positions but oriented parallel, the cLEOD showed the usual head-to-tail pattern (Fig. 6B,C). The second example is shown in Fig. 7B (black top trace). In this case, the two fish were parallel and close to each other with their snouts at the same level. The cLEOD recorded under these conditions was more similar to the sLEOD than to the htEOD [cV_1 was relatively larger than V_2 (arrowhead in top trace of Fig. 7B), cV_2 was absent and cV_4 was almost absent (asterisk in top trace of Fig. 7B)].

Differences between the sLEOD and cLEOD at the electroreceptive fovea

Clear differences between sLEOD and cLEOD at the electroreceptive fovea were apparent in their time waveforms (Fig. 10). (i) The ratio sV_1/sV_3 was five times larger than the ratio cV_1/cV_3 (Fisher exact test, $P<0.001$, $N=25$). (ii) In 80 % of the specimens studied, the sLEOD lacked the sharp negative

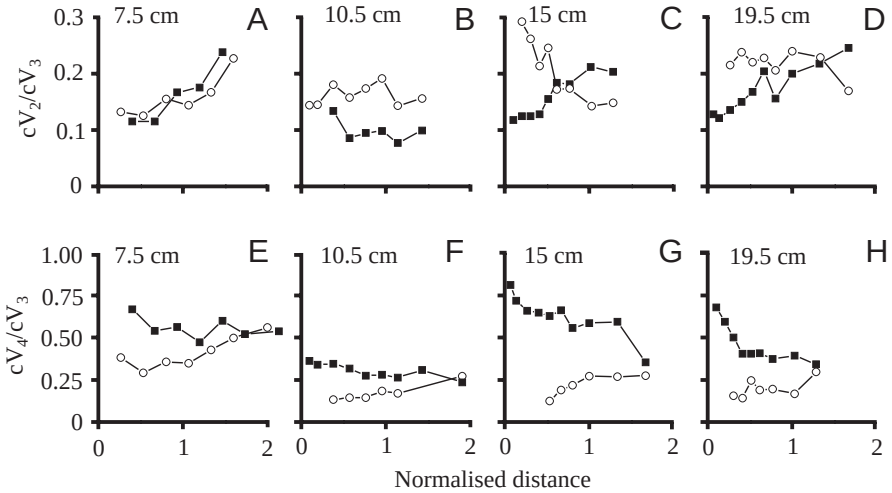

Fig. 9. The time waveform of the conspecific-generated local electric-organ-discharge-associated field (cLEOD) depends on the distance, size and orientation of the emitter fish. Data obtained from the same fish as in Fig. 8 (the emitting fish ranged from 7.5 to 19.5 cm in length, the receiving fish was 12 cm long). (A–D) The ratio cV_2/cV_3 as a function of distance between fish (normalised to the length of the emitting fish). (E–H) The ratio cV_4/cV_3 as a function of distance between fish (normalised to the length of the emitting fish). (○) Fish in parallel orientation; (■) fish in anti-parallel orientation. For an explanation of the nomenclature, see Fig. 1.

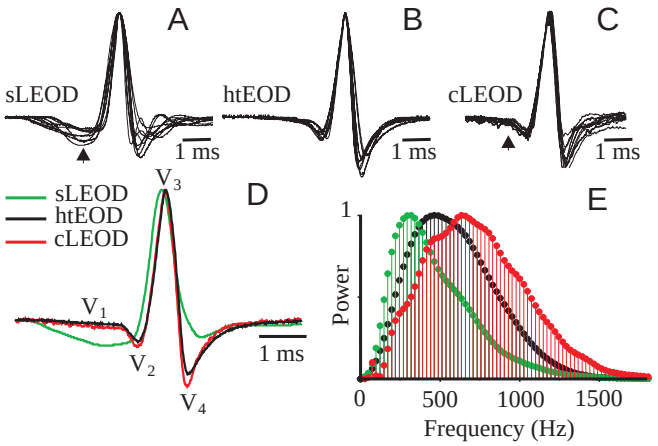

Fig. 10. Differences between the foveal self-generated local electric-organ-discharge-associated field (sLEOD), the foveal conspecific-generated local electric-organ-discharge-associated field (cLEOD) and the head-to-tail electric-organ-discharge-associated field (htEOD) time waveforms. Each trace is the average of eight sweeps. (A) Traces of the normalised sLEOD generated by 10 different fish (ranging in length from 7 to 24 cm). (B) Traces of the normalised htEOD obtained from the same 10 fish as in A. (C) Traces of the normalised cLEOD generated by 10 other emitting fish (emitting fish ranging in length from 7 to 24 cm, receiving fish 12 cm long). Note that superimposed traces shown in A, B and C were aligned and normalised to the peak of V_3. The relative amplitude of V_1 mentioned in the text was measured 1.3 ms before the peak of V_3 (arrowheads in A and C). (D) Normalised time waveforms for the sLEOD (green), htEOD (black) and cLEOD (red) generated by a 22 cm emitting fish; the cLEOD was recorded at the fovea of a parallel 14 cm long fish, 10 cm away. (E) Normalised power spectral density histograms corresponding to the waveforms in D (same colour coding).

component corresponding to cV_2 and V_2; in the other 20 %, it was only present as a small notch. (iii) sV_3 lasted longer and occurred 0.3 ms before cV_3 (Fig. 10D). (iv) Despite its dependence on the relative distance, orientation and size of the emitting fish, cV_4 was the second largest component after cV_3. In contrast with this large cV_4, sV_4 was very small and present in only 60 % of the studied specimens. (v) Between-fish variability of the sLEOD was higher than variability of the cLEOD except for the late components (sV_4 and cV_4). (vi) The slope between cV_3 and cV_4 was often steeper than the slope between sV_3 and sV_4. These slopes are represented by the high-frequency flank in the power spectral density histograms. Consequently, although the cLEOD and htEOD power spectral densities were similar, the mean peak frequency of the former was often shifted to higher frequencies (Fig. 10E; the spectral peak of the cLEOD was at 570±105 Hz, N=10, parallel orientation; the spectral peak of the htEOD was at 517±96 Hz, N=10; unpaired t-test, P<0.001; means ± S.D.). (vii) Consistent with the greater relative importance of the early component (sV_1) and the longer duration of sV_3, the peak of the power spectral density of the sLEOD occurred at lower frequencies than the peaks of the power spectral densities of both the cLEOD and the htEOD (Fig. 10E; the spectral peak of the sLEOD was at 355±86 Hz; mean ± S.D., N=10; differences between the sLEOD and htEOD were statistically significant; paired t-test, P<0.001).

A second type of difference between foveal sLEODs and cLEODs was their amplitude-dependence on emitter fish length. The amplitude of the sLEOD at the fovea was linear and decreasing function of fish length (Fig. 11A; for sV_1, r=0.8, P<0.001; for sV_3, r=0.92, P<0.001; N=16). Interestingly, despite the wide range of fish lengths used, no differences were found in the vector angles of the sLEOD at the fovea. In contrast to the sLEOD, the amplitude of the cLEOD was a linear and increasing function of emitter fish length (Fig. 11B; cV_3, r=0.92, P<0.001, N=14). The amplitude of the htEOD also increased with fish length (Fig. 11C; V_3, r=0.83, P<0.001, N=27).

Relative importance of regional EODs for the sLEOD and cLEOD

To study the origins of the sLEOD and cLEOD, different regions of the electric organ were silenced surgically. Spinal section was employed to abolish the trunk discharge ('trunk-silenced' fish, N=5) and surgical resection of the abdominal portion of the electric organ was employed to abolish the abdominal discharge ('abdomen-silenced' fish, N=5; see Materials and methods for details).

The sLEOD of an 'abdomen-silenced' fish was smaller than and different in waveform from the control sLEOD. The sLEOD of an 'abdomen-silenced' fish was qualitatively similar to the cLEOD, showing a 90 % reduction in sV_1 (similar to the reduction in abdominal electromotive force) but only a 70 % reduction in sV_3. A sharp negative wave (sV_2) preceding sV_3

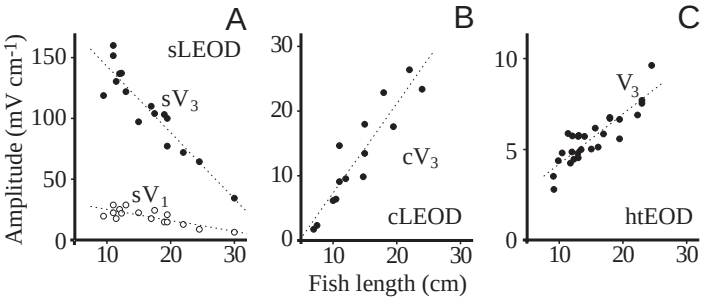

Fig. 11. Amplitude of the foveal self-generated local electric-organ-discharge-associated field (sLEOD) (A), of the conspecific-generated local electric-organ-discharge-associated field (cLEOD) (B) and of the head-to-tail electric-organ-discharge-associated field (htEOD) (C) as functions of the length of the emitting fish. In the case of the sLEOD, the peak of the two principal components is plotted (sV_3 ●, sV_1 ○). Note that sV_1 and sV_3 of the sLEOD decrease with fish length, whereas cV_3 of the cLEOD and V_3 of the htEOD increase with fish length. For an explanation of the nomenclature, see Fig. 1. Suffixes 's' and 'c' indicate self- and conspecific-generated fields, respectively.

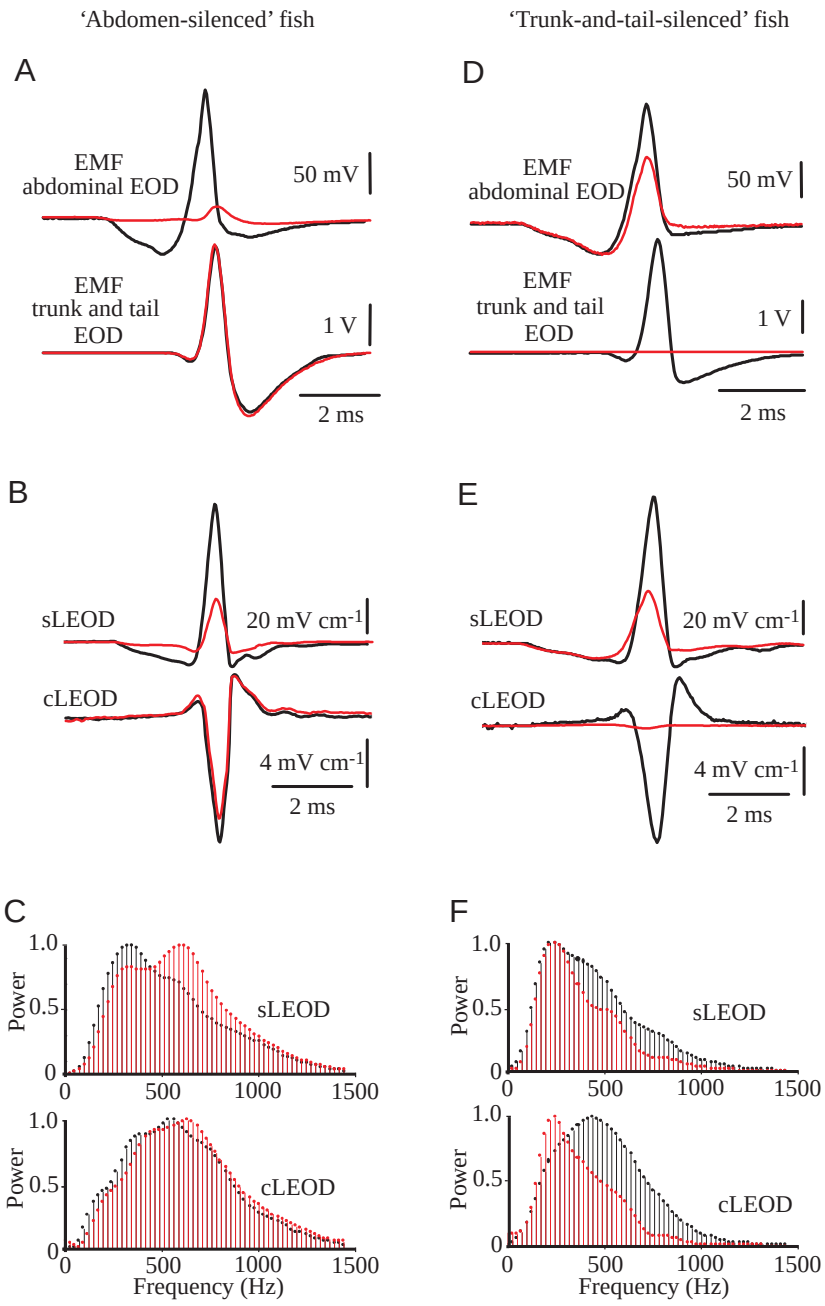

Fig. 12. The relative importance of the discharges of different regions of the electric organ on the self-generated local electric-organ-discharge-associated field (sLEOD) and the conspecific-generated local electric-organ-discharge-associated field (cLEOD) explored by lesion experiments. Each trace is the average of eight sweeps. For an explanation of the nomenclature, see Fig. 1; suffixes 's' and 'c' indicate self- and conspecific-generated fields respectively. The left-hand column (A–C) compares recordings made before (black) and after (red) surgical ablation of the abdominal region of the electric organ. Note in A that the electromotive force (EMF) generated at the abdominal region (top traces) was dramatically decreased, whilst it remained unchanged at the trunk and tail (bottom traces). The top traces in B show that abdominal lesion almost abolished sV_1 whilst sV_3 decreased in amplitude to approximately one-third. Overall, the sLEOD waveform became similar to the head-to-tail electric-organ-discharge-associated field (htEOD) waveform. Consistent with this, the peak of the sLEOD power spectral density histogram (the top of C) approached that of the cLEOD. Almost no changes were observed in the cLEOD following ablation of the abdominal region of the electric organ (bottom traces in B and bottom histogram in C). The right-hand column (D–F) compares recordings made before (black) and after (red) spinal section at 35% along the fish's body. Spinal section silenced the trunk and tail regions of the electric organ and diminished V_3 in the abdominal region (D). No changes were observed in sV_1, but important changes were observed in the fast deflections of the sLEOD (E). In accordance with the changes in sV_3, a decrease in the right flank of the sLEOD histogram (top of F) was observed. The bottom traces in E show that the cLEOD was practically abolished. Furthermore, the remnant cLEOD waveform was similar to that of the sLEOD, with the peak of the power spectrum density histogram (bottom of F) shifted to a lower frequency range.

was apparent, and the ratio sV_4/sV_3 increased. Consistent with the dramatic reduction in sV_1, the smaller decrease in sV_3 and the relative increase in sV_2 and sV_4, the power spectral density of the sLEOD was shifted to a higher frequency range (Fig. 12A–C). In contrast, the time waveform and power spectral density of the cLEOD generated by 'abdomen-silenced' fish on the skin of a conspecific remained almost unchanged (Fig. 12B,C).

The sLEOD of a 'trunk-silenced' fish was qualitatively similar to the control sLEOD (Fig. 12E). However, while sV_1 was identical to the control, the amplitude of sV_3 diminished to 36% of the control. This decrease was larger than the decrease observed in the trunk and tail electromotive force (remnant of trunk and tail sV_3, 57% of the control). In the example in Fig. 12E, a small sV_2 was observed in the control condition. This component disappeared after spinal section. Consistent with the decrease in sV_3, the power in the high-frequency region of the spectral density of the sLEOD decreased compared with the control (Fig. 12F, upper graph). The cLEOD generated by the 'trunk-silenced' fish on the skin of a conspecific was more than 15 times smaller. In addition, the power spectral density of the cLEOD was shifted to lower frequencies and resembled the power spectral density of the sLEOD (Fig. 12E,F).

These findings show (i) the relative importance of the abdominal EOD as a source of the sLEOD; (ii) the relative unimportance of abdominal EOD as a source of the cLEOD; (iii) the relative importance of the trunk and tail EOD as a source of the cLEOD; and (iv) the relative unimportance of the

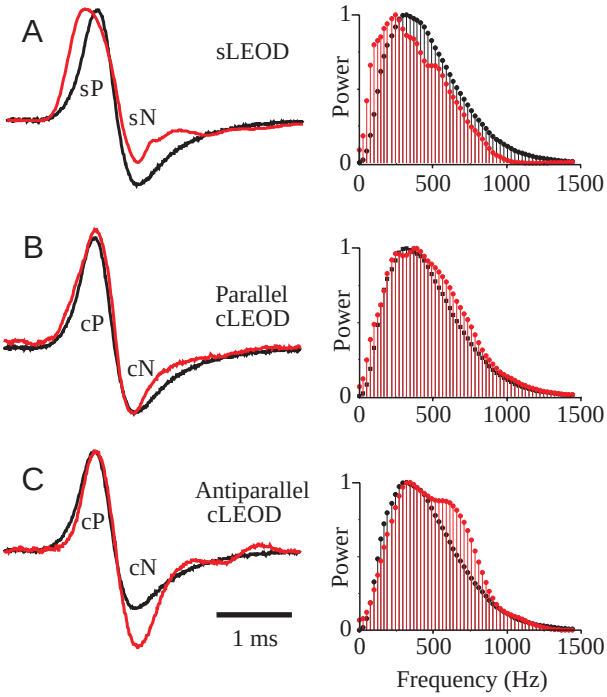

Fig. 13. The self-generated local electric-organ-discharge-associated field (sLEOD), the conspecific-generated local electric-organ-discharge-associated field (cLEOD) and the head-to-tail electric-organ-discharge-associated field (htEOD) time waveforms and power spectral densities of *Brachyhypopomus pinnicaudatus*. Each trace is the average of eight sweeps. Time waveforms are presented on the left and power spectral density histograms on the right. (A) The foveal sLEOD (red) and htEOD (black) from a 17 cm long male. (B) The cLEOD (red) generated by a 17 cm long male emitting fish at the fovea of a 20 cm long male receiving fish placed 7 cm away from and parallel to the emitting fish. The htEOD of the emitting fish is shown for comparison (black). (C) Same two fish as in B, but in the anti-parallel orientation, with the fish separated by 7 cm. The cLEOD is shown in red and the htEOD at the emitting fish in black (cP, the initial positive component; cN, the later negative component).

trunk and tail EOD as a source of the sLEOD. Nevertheless, the decrease in the sV_1/sV_3 ratio in 'abdomen-silenced' fish and the increase in the sV_1/sV_3 ratio in 'trunk-and-tail-silenced' fish indicate that sV_3 is generated not only by abdominal sources. The present data suggest that approximately two-thirds of sV_3 is generated by the abdominal region whilst the rest is generated more caudally.

Data obtained from B. pinnicaudatus

As comparative data, the sLEOD and the cLEOD were recorded in two specimens of *B. pinnicaudatus*. These fish show a biphasic htEOD with an initial positive component (P) and a later negative component (N). We use similar nomenclature for the corresponding components of the sLEOD and cLEOD. Fig. 13 compares normalised waveforms and power spectra of the foveal sLEOD and cLEOD (red traces) with the htEOD (black traces).

In this species, the sLEOD showed a longer sP wave and a rather smaller sN wave than the P and N waves of the htEOD (Fig. 13A). This confirms previous data (Stoddard et al., 1999) for different species of *Brachypopomus*. The relative unimportance of the N component in sLEOD at the head region must be due to its caudal origin (Caputi et al., 1998b).

As in *G. carapo*, the cLEOD waveform of *B. pinnicaudatus* was very similar to the htEOD waveform when the fish were either parallel (Fig. 13B) or antiparallel (Fig. 13C). The cN/cP ratio was larger than the head-to-tail N/P ratio. The largest cN/cP ratio occurred when the fish were anti-parallel (Fig. 13C). According to these differences in waveform, the power spectrum of the sLEOD was shifted to lower frequencies compared with the power spectrum of the htEOD (Fig. 13A right), and the differences between the cLEOD and htEOD power spectra only occurred at the high-frequency flank (right-hand parts of Fig. 13B,C).

Discussion

The sLEOD and the organisation of the active electrolocation field

Examination of self-generated local electric fields (sLEOD) at the foveal/parafoveal region of *G. carapo* showed two main wave components (sV_1 and sV_3). In these regions, the time waveform was site-independent, showing variations only in amplitude. Vector angles were time-independent, as expected for a non-contiguous electric source. The coherent and radially collimated sV_1–sV_3 local field was modulated by nearby objects (Fig. 4), so it can be postulated that these wave components are carriers for the active electrolocation signals sensed at the foveal/parafoveal region.

The characteristics of this strong, coherent and collimated carrier are well suited to yield high-resolution physical images to match the high-density array of various types of electroreceptor present at the fovea (types I and II; Szabo, 1974; Echagüe and Trujillo-Cenóz, 1980). First, local amplitude modulation of a relatively strong carrier will cause a large contrast-to-noise ratio at the level of the receptive surface. Second, a collimated local field narrows the receptive field for each electroreceptor, thereby increasing spatial resolution. In addition, perpendicularity between the local field and the skin increases the directional efficiency of transcutaneous currents as stimuli for electroreceptors. This effect can be considered analogous to the Stiles–Crawford effect in vision (Buser and Imbert, 1987). Third, it has been shown that changes in waveform produced by an object's impedance may encode a perceptual quality, much as wavelength encodes colour in vision (von der Emde, 1990; Budelli and Caputi, 2000). So, waveform coherence and the variety of receptor types at the fovea are well suited to support an impedance-related, or 'electric colour', discrimination, further increasing the resolution of the image.

Caudal to the head, sLEODs waveforms were not alike, and vector angles changed over time. This is a consequence of the activation of a spatially extended, structurally heterogeneous electric generator (see below). This suggests that the weak,

non-coherent and non-collimated sLEODs occurring at the trunk and tail should yield a blurred image, which matches the low density and poor variety of electroreceptor types in these regions.

Differences between the sLEOD and cLEOD are based on their different origins

The experimental data reported here provide evidence that the local electric fields generated by the EOD of an emitting *Gymnotus carapo* have different waveforms when recorded close to its own skin (sLEOD) or close to the skin of a potentially receptive conspecific (cLEOD). Note that each fish can be considered both as a receiver of its own EOD and as a receiver of the electric signals from a neighbouring conspecific.

The differences between the sLEOD and the cLEOD can be explained on the basis of the mechanisms of generation of the EOD waveform, the filtering properties of bodies of the emitting and receiving fish, and the physical properties of electric fields. Our results indicate that the sLEOD and the cLEOD contain different proportions of the wave components that are generated by different regions of the electric organ. Experiments using specimens with silenced regions of the electric organ showed that the foveal sLEOD is mainly generated by the fish's own abdominal region. The foveal cLEOD in a receiving fish is mainly generated at the trunk and tail regions of the emitting fish (with the exception of cLEODs generating by a nearby fish whose abdominal region overlaps that of the receiving fish; Figs 6, 7). However, both sLEODs and cLEODs recorded at the trunk or tail (the low-resolution electroreceptive zones) are generated by the trunk and tail regions.

The abdominal region generates a low electromotive force, and its internal resistance is also low because of the shape of the fish (see Caputi, 1999). The abdominal region of the fish therefore acts as a 'voltage source', in which current is more dependent on load than voltage (Donaldson, 1958). As a consequence, the transcutaneous current density generated by such a source (which is proportional to the transcutaneous voltage) must be strongly affected by the impedance of nearby objects. This would be required for electric imaging in active electrolocation. In addition, the V_1–V_3 fields resulting from activation of the abdominal region of the electric organ have a small equivalent dipole and are virtually restricted to the close environment as a consequence. Therefore, these fields are not good candidates for carrying communication signals, except in the case of fish that are very close to each other.

In contrast, the trunk and tail region appear well suited for generating the electrocommunication signal carrier. The electromotive force and internal resistance of the trunk and tail regions are relatively high (up to 10 times the values in the abdominal region; Caputi et al., 1989; Caputi and Budelli, 1995). In addition, this region is approximately six times longer than the abdominal region. Thus, the trunk and tail regions of the electric organ act more as a 'current source' and have a much stronger equivalent dipole than the abdominal region. These features are necessary to generate the strong fields at longer distances required for long-range electrocommunication.

Interestingly, the strong discharges emitted caudally are relatively unimportant in the sLEOD recorded at the fovea. This probably derives from the shape of the fish. Currents flowing along the body of the fish will increase with the ratio of skin resistance to internal resistance, which is in turn proportional to the mean transverse diameter of the fish (Caputi and Budelli, 1995). The large diameter of the rostral third of the body facilitates current flow from the abdominal region to the rostral pole. Conversely, the small diameter of the caudal region of the body presents an obstacle for rostral propagation of wave components originating in the tail. Because of the monotonic decrease in diameter along the tail, this effect is more pronounced the more caudally located the generator; thus, the least facilitated component is the tail complex V_3–V_4.

It is important to note that, beyond some critical distance from a heterogeneous electric source, the associated field becomes similar to the field generated by a dipole with an equivalent waveform (Nunez, 1981). This may explain the general finding that cLEOD waveforms recorded at the fovea of conspecifics are similar to the htEOD of the emitter fish. However, when fish are close, the relative importance of regional waveforms becomes orientation-dependent. Anti-parallel fish generate a large cV_4 at the fovea of the receiving fish because the generator of this component (the tail of the emitter fish) is the nearest. Consistent with this, parallel fish produce a relatively small cV_4 but a relatively large cV_2. Moreover, when fish are almost touching, a cV_1 was sometimes apparent. When the emitter fish was rather smaller than the receiving fish, cV_2/cV_3 increased with the distance between the fish in both parallel and anti-parallel orientations. These arguments suggest that information about the emitter's size, orientation and distance could be extracted from the spatial patterns and relative magnitudes of the cLEOD components.

While the cLEOD increased as a function of fish length, the sLEOD decreased. These opposite scaling effects can be explained by the physics of electric field generation. The increase in the cLEOD amplitude with the length of the emitter fish results from the increased power of the equivalent source and the longer arm of the equivalent dipole (Caputi et al., 1989). The decrease in the sLEOD as fish size increases must be due to a decrease in the surface area/volume ratio (Caputi and Budelli, 1995).

Possible significance of the differences between the sLEOD and cLEOD waveforms

A comparison of LEOD waveform Fourier analysis with the known tuning properties of electroreceptors (Bastian, 1976; Bastian, 1977; Bastian, 1986; Watson and Bastian, 1979; Zakon, 1986; McKibben et al., 1993; Yager and Hopkins, 1993) leads us to speculate that electrocommunication and active electrolocation signals may be partially segregated by the differences between their carriers. Low-pass electroreceptors are not likely to be stimulated by low-amplitude cLEODs, which peak at much higher frequencies

than their best-frequency response, but are probably stimulated by large-amplitude sLEODs, which have most of their power in the low-frequency band. Because of the differences in amplitude (the sLEOD can be up to 75 times larger than the cLEOD), wide-band receptors should respond better to the sLEOD than to the cLEOD. Finally, narrow-band electroreceptors, whose best frequency responses are close to the peak of the cLEOD power spectral density histogram, may be maximally stimulated by the cLEOD. These receptors should also be stimulated by the sLEOD since the absolute power of the cLEOD at the peak of its spectrum is no larger than the absolute power of the sLEOD within the same frequency range. In agreement with this hypothesis, we found that both the sLEOD and the cLEOD evoke the same kind of oscillations as described previously (Watson and Bastian, 1979) for this type of receptor (Figs 3, 5B, 12B). We speculate that narrow-band electroreceptors may subserve both electrolocation and electrocommunication, whereas wide-band and low-frequency electroreceptors are more likely to subserve active electrolocation. Nevertheless, the present results do not rule out the possibility that slow components of the cLEOD waveform, occurring when two relatively large fish are close together, may have enough amplitude to play a role in electrocommunication (see examples in Figs 6, 7).

In *B. pinnicaudatus*, which exhibits similar types of electroreceptor (Bastian, 1976; Bastian, 1977), we found that the power spectrum of the sLEOD peaks at lower frequencies than that of cLEOD. This suggests that a similar strategy for separating electrolocation and electrocommunication signals might be present in this species.

Environmental factors and endocrine signals modulate V_4 in *G. carapo* and N in *B. pinnicaudatus* (Hopkins et al., 1990; Caputi et al., 1998b; Franchina and Stoddard, 1998; Silva et al., 1999; J. L. Ardanaz, and O. Macadar, personal communication). Such modulation relates to conspecific sex identification (Schumway and Zellick, 1988). These wave components, which are generated in the tail region, are prominent in the cLEOD but barely present in the sLEOD. Modulation of cLEOD variables without affecting sLEOD variables in the high-resolution sensory area might be a good strategy for sending sexual signals without adversely affecting active electrolocation.

The authors thank Professor O. Trujillo-Cenóz for his valuable critical comments on the manuscript. This research was partially funded by Proyecto Premio Clemente Estable 4014 and a PEDECIBA doctorate studentship to P.A.

References

Assad, C., Rasnow, B. and Stoddard, P. K. (1999). Electric organ discharges and electric images during electrolocation. *J. Exp. Biol.* **202**, 1185–1193.

Bastian, J. (1976). Frequency response characteristics of electroreceptors in weakly electric fish (Gymnotidei) with a pulse discharge. *J. Comp. Physiol.* A **112**, 165–180.

Bastian, J. (1977). Variations in the frequency response of electroreceptors dependent on receptors location in weakly electric fish (Gymnotidei) with a pulse discharge. *J. Comp. Physiol.* A **121**, 53–64.

Bastian, J. (1986). Electrolocation: Behavior, anatomy and physiology. In *Electroreception* (ed. T. H. Bullock and W. Heiligenberg), pp. 577–612. New York: Wiley.

Bennett, M. V. L. (1971). Electric organs. In *Fish Physiology*, vol. V (ed. W. S. Hoar and D. J. Randall), pp. 347–491. New York: Wiley.

Black-Cleworth, P. (1970). The role of electrical discharges in the non-reproductive social behavior of *Gymnotus carapo* (Gymnotidae, Pisces). *Anim. Behav. Monogr.* **3**, 1–77.

Budelli, R. and Caputi, A. A. (2000). The electric image in weakly electric fish: perception of objects of complex impedance. *J. Exp. Biol.* **203**, 481–492.

Buser, P. and Imbert, M. (1987). *Neurophysiologie Functionelle*, vol. IV, *Vision*, 469p. Paris: Hermann.

Caputi, A. A. (1999). The EOD of pulse gymnotiforms, from a single impulse to a complex electromotor pattern. *J. Exp. Biol.* **202**, 1229–1241.

Caputi, A. and Budelli, R. (1995). The electric image in weakly electric fish. I. A data-based model of waveform generation in *Gymnotus carapo*. *J. Comput. Neurosci.* **2**, 131–147.

Caputi, A. A., Budelli, R., Grant, K. and Bell, C. C. (1998a). The electric image in weakly electric fish. Physical images of resistive objects in *Gnathonemus petersii*. *J. Exp. Biol.* **201**, 2115–2128.

Caputi, A., Macadar, O. and Trujillo-Cenóz, O. (1989). Waveform generation in *Gymnotus carapo*. III. Analysis of the fish body as an electric source. *J. Comp. Physiol.* A **165**, 361–370.

Caputi, A., Macadar, O. and Trujillo-Cenóz, O. (1994). Waveform generation in *Rhamphichthys rostratus* (L.) (Teleostei, Gymnotiformes). The electric organ and its spatiotemporal activation pattern. *J. Comp. Physiol.* A **174**, 633–642.

Caputi, A., Silva, A. and Macadar, O. (1993). Electric organ activation in *Gymnotus carapo:* spinal and peripheral mechanisms. *J. Comp. Physiol.* A **173**, 227–232.

Caputi, A. A., Silva, A. and Macadar, O. (1998b). The effect of environmental variables on waveform generation in *Brachyhypopomus pinnicaudatus*. *Brain Behav. Evol.* **52**, 148–158.

Caputi, A. and Trujillo-Cenóz, O. (1994). The spinal cord of *Gymnotus carapo*: the electromotorneurons and their projection pattern. *Brain Behav. Evol.* **44**, 166–174.

Castelló, M. E., Aguilera, P. A., Trujillo-Cenóz, O. and Caputi, A. A. (2000) Electroreception in *Gymnotus carapo*: pre-receptor mechanisms and distribution of electroreceptor types. *J. Exp. Biol.* **203**, 3279–3287.

Castelló, M. E., Caputi, A. and Trujillo-Cenóz, O. (1998). Structural and functional aspects of the fast electrosensory pathway in the electrosensory lateral line lobe of the pulse fish *Gymnotus carapo*. *J. Comp. Neurol.* **401**, 549–563.

Donaldson, P. E. K. (1958). *Electronic Apparatus for Biological Research*. London: Butterworth.

Echagüe, A. and Trujillo-Cenóz, O. (1980). Innervation patterns in the tuberous organs of *Gymnotus carapo*. In *Sensory Physiology of Aquatic Lower Vertebrates* (ed. T. Szabó and G. Czéh). *Adv. Physiol. Sci.* **31**, 29–40. Budapest: Pergamon Press.

Franchina, C. R. and Stoddard, P. K. (1998). Plasticity of the electric organ discharge waveform of the electric fish *Brachypopomus pinnicaudatus.* I. Quantification of day–night changes. *J. Comp. Physiol.* A **183**, 759–768.

Hopkins, C. D. (1991). *Hypopomus pinnicaudatus* (Hypopomidae),

a new species of gymnotiform fish from French Guiana. *Copeia* **1**, 151–161.

Hopkins, C. D., Comfort, N., Bastian, J. and Bass, A. H. (1990). Functional analysis of sexual dimorphism in an electric fish *Hypopomus pinnicaudatus*. *Brain Behav. Evol.* **35**, 350–367.

Lissmann, H. W. and Machin, K. E. (1958). The mechanism of object location in *Gymnarchus niloticus* and similar fish. *J. Exp. Biol.* **35**, 451–486.

Marr, D. (1982). *Vision.* New York: Freeman.

McKibben, J. R., Hopkins, C. D. and Yager, D. D. (1993). Directional sensitivity of tuberous electroreceptors: Polarity preferences and frequency tuning. *J. Comp Physiol.* A **173**, 415–424.

Nunez, P. (1981). *Electric Fields of the Brain. The Neurophysics of EEG*. New York, Oxford: Oxford University Press.

Rasnow, B. and Bower, J. M. (1996). The electric organ discharges of the gymnotiform fishes. I. *Apteronotus leptorhynchus. J. Comp. Physiol.* A **178**, 383–396.

Schumway, C. A. and Zelick, R. D. (1988). Sex recognition and neural coding of electric organ discharge waveform in the pulse type weakly electric fish. *Hypopomus occidentalis. J. Comp. Physiol.* A **163**, 465–478.

Sicardi, A. E., Caputi, A. A. and Budelli, R. (2000). Physical basis of distance discrimination. *Physica A* (in press).

Silva, A., Quintana, L., Galeano, M., Errandonea, P. and Macadar, O. (1999). Temperature sensitivity of the EOD of *Brachyhypopomus pinnicaudatus* in the wild and under captivity. *J. Comp. Physiol.* A **185**, 187–197.

Stoddard, P. K., Rasnow, B. and Assad, C. (1999). Electric organ discharge of the gymnotiform fishes. III. *Brachyhypopomus*. *J. Comp. Physiol.* A **184**, 609–630.

Szabo, T. (1974). Anatomy of the specialised lateral line organs of electroreception. In *Handbook of Sensory Physiology*, vol. III/3 (ed. A. Fessard), pp. 13–58. Berlin: Springer-Verlag.

Trujillo-Cenóz, O., Echagüe, J. A. and Macadar, O. (1984). Innervation pattern and electric organ discharge waveform in *Gymnotus carapo*. *J. Neurobiol*. **15**, 273–281.

von der Emde, G. (1990). Discrimination of objects through electrolocation in weakly electric fish, *Gnathonemus petersii*. *J. Comp. Physiol*. A **167**, 413–421.

Watson, D. and Bastian, J. (1979). Frequency response characteristics of electroreceptors in the weakly electric fish *Gymnotus carapo*. *J. Comp. Physiol.* A **134**, 191–202.

Wiener, N. (1948). *Cybernetics: or Control and Communication in the Animal and the Machine.* Cambridge, MA: The MIT press.

Yager, D. D. and Hopkins, C. D. (1993). Directional characteristics of tuberous electroreceptors in the weakly electric fish *Hypopomus* (Gymnotiformes). *J. Comp. Physiol.* A **143**, 401–414.

Zakon, H. H. (1986). The electroreceptive periphery. In *Electroreception* (ed. T. H. Bullock and W. Heiligenberg), pp. 577–612. New York: Wiley.